
HOKKAIDO UNIVERSITY

Title	Magneto-optical investigation of epitaxial nonstoichiometric Co2MnGe thin films
Author(s)	Trudel, Simon; Hamrle, Jaroslav; Hillebrands, Burkard; Taira, Tomoyuki; Yamamoto, Masafumi
Citation	Journal of Applied Physics, 107(4), 043912 https://doi.org/10.1063/1.3296350
Issue Date	2010-02-15
Doc URL	http://hdl.handle.net/2115/42761
Rights	Copyright 2010 American Institute of Physics. This article may be downloaded for personal use only. Any other use requires prior permission of the author and the American Institute of Physics. The following article appeared in J. Appl. Phys. 107, 043912 (2010) and may be found at https://dx.doi.org/10.1063/1.3296350
Type	article
File Information	JAP107-4_043912.pdf


Instructions for use

Hokkaido University Collection of Scholarly and Academic Papers : HUSCAP

Magneto-optical investigation of epitaxial nonstoichiometric Co_2MnGe thin films

Simon Trudel,[1,a)] Jaroslav Hamrle,[1] Burkard Hillebrands,[1] Tomoyuki Taira,[2] and Masafumi Yamamoto[2]
[1]*Fachbereich Physik and Forschungszentrum OPTIMAS, Technische Universität Kaiserslautern, Erwin-Schrödinger-Straße 56, D-67663 Kaiserslautern, Germany*
[2]*Division of Electronics for Informatics, Graduate School of Information Science and Technology, Hokkaido University, N14, W9, Kita-ku, Sapporo 060-0814, Japan*

(Received 9 October 2009; accepted 16 December 2009; published online 25 February 2010)

We investigate the magneto-optical properties of a nonstoichiometric, epitaxial $Co_2Mn_{0.77}Ge_{0.42}(001)$ film grown on a MgO-buffered MgO(001) single-crystal substrate. Magneto-optical Kerr effect magnetometry indicates that the sample has strong uniaxial anisotropy, whereas the easy and hard axes of magnetization are tilted by $\sim 10°$ with respect to the [110] and $[1\bar{1}0]$ directions, respectively. A modest quadratic Kerr effect with an amplitude of 0.4 mdeg was observed. Brillouin light scattering spectroscopy was used to find that the exchange constant A, spin-wave stiffness D, and saturation magnetization M_s are 22.5 pJ/m, 413 meV Å^2, and 6.43 μ_B/f.u., respectively. The saturation magnetization value suggests that the Slater–Pauling rule might apply to such nonstoichiometric compositions. © *2010 American Institute of Physics*. [doi:10.1063/1.3296350]

I. INTRODUCTION

Co_2MnGe, as many other Co_2-based Heusler compounds (Co_2MZ, where M is a transition metal and Z is a main group element), is attracting considerable attention due to its predicted half-metallicity.[1–4] Materials endowed with this property support a particular band structure in which the majority-spin channel is metallic, whereas the minority spin channel is semiconducting. In theory, this provides a 100% spin polarization at the Fermi level, which is attractive for spintronic applications. For Co_2MnGe, the Fermi level lies near the middle of the minority spin band gap.[2] This is advantageous for conserving half-metallicity at finite temperatures or in the presence of defects which smear the electron density near the valence or conduction bands. Futhermore, Co_2MnGe boasts a high Curie temperature of 905 K,[5] which is a prerequisite for implementation in practical devices. It also features a small lattice mismatch of −3.6% between Co_2MnGe and MgO [after a 45° in-plane rotation within the (001) plane, see Fig. 1], compared to, for example, that of −5.1% between Co_2MnSi and MgO. This small mismatch is not only preferable for realizing high-performance magnetic tunnel junctions (MTJs) with potentially half-metallic Heusler-compound electrodes but also to build layered structures for spin-injection from a Heusler-compound electrode into semiconductors through a MgO barrier.

Some of the present authors recently developed fully epitaxial MgO-based MTJs wherein a Heusler-compound thin film serves as either the lower or both the lower and upper ferromagnetic electrodes.[6–10] Relatively high tunnel magnetoresistance (TMR) ratios of 376% at 4.2 K and 160% at room temperature (RT) were reported for $Co_2MnGe/MgO/Co_{50}Fe_{50}$ MTJs with a Mn- and Ge-deficient $Co_2Mn_{0.77}Ge_{0.42}$ lower electrode.[11,12] Furthermore, high TMR ratios of 1135% at 4.2 K and 236% at RT were demonstrated for $Co_2MnSi/MgO/Co_2MnSi$ MTJs with Mn-rich $Co_2Mn_{1.29}Si$ electrodes.[13]

It was recently shown that the temperature dependence of the TMR ratio of a $Co_2FeAl_{0.5}Si_{0.5}/MgAl_2O_x/CoFe$ TMJ followed a $T^{3/2}$ power law (T being the temperature), due to the thermal excitation of spin waves.[14] Furthermore, for fully epitaxial Co_2MZ/MgO-based MTJs, including $Co_2MnSi/MgO/Co_{50}Fe_{50}$,[8] $Co_2Cr_{0.6}Fe_{0.4}Al/MgO/Co_{50}Fe_{50}$,[15] and $Co_2MnSi/MgO/Co_2MnSi$ (Ref. 16) junctions, the tunnel resistance for the parallel magnetization configuration were almost independent of temperature from 4.2 to 300 K, while that for the antiparallel magnetization configuration (R_{AP}) were strongly dependent on T and decreased with increasing T. This strong temperature dependence of R_{AP} was also dis-

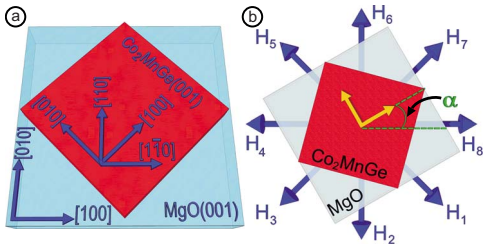

FIG. 1. (Color online) (a) Epitaxial relation between the MgO buffered MgO(001) substrate and the Co_2MnGe film. The Co_2MnGe film grows with a (001) orientation, and the edges of its cubic unit cell are rotated by an in-plane angle of 45° with respect to the edges of the MgO unit cell, i.e., $Co_2MnGe(001)[100]\|MgO(001)[110]$. (b) Geometry of the MOKE measurements. The eight fields are those used for the QMOKE measurements in saturation (see text). The plane of light incidence contains $\mathbf{H}_4$, $\mathbf{H}_8$, and the sample's normal, and forms an angle α with the edge of the sample (i.e., an MgO[100] direction).

a)Present address: Department of Chemistry, University of Calgary, 2500 University Dr. NW, Calgary, Alberta T2N 1N4, Canada; Electronic mail: Email: trudels@ucalgary.ca.

 © 2010 American Institute of Physics

Downloaded 15 Mar 2010 to 133.87.26.32. Redistribution subject to AIP license or copyright; see http://jap.aip.org/jap/copyright.jsp

cussed in terms of the role of thermally excited magnons for spin-flip scattering[17] from the majority-spin band to minority spin gap states, including minority spin interface states, in the emitter electrode, and vice versa in the collector electrodes.[16,18] In this context, the knowledge of the exchange stiffness, which will largely determine the energy required to create a spin wave, is a crucial parameter that must be understood to gain insight into the construction of superior devices.

As a part of our ongoing investigation of the magneto-optical properties of Co_2-based Heusler compounds by means of magneto-optical Kerr effect (MOKE) magnetometry[19–23] and Brillouin light scattering (BLS) spectroscopy,[19,24–26] we here report on the investigation of the Mn- and Ge-deficient, nonstoichiometric epitaxial $Co_2Mn_{0.77}Ge_{0.42}$ films described above. The compound of interest here, Co_2MnGe, was recently investigated by BLS spectroscopy.[27,28] However, in that study, $Co_2MnGe(110)$ films were grown by rf-sputtering onto V-buffered *a*-plane Al_2O_3, and the actual stoichiometry was not verified. We show the exchange constant is nearly doubled for our nonstoichiometric $Co_2Mn_xGe_y$ $(x,y<1)$ thin films compared to that reported for the $Co_2MnGe(110)$ films.[27,28]

II. SAMPLE PREPARATION AND CHARACTERIZATION

A. Sample preparation and structural details

The nominal studied sample layer structure was as follows: MgO(001) substrate/MgO buffer (10 nm)/Co_2MnGe (50 nm)/MgO barrier (2 nm)/AlO_x capping layer (1 nm). The sample was prepared in an ultrahigh vacuum chamber maintained at a base pressure of $\sim 6\times 10^{-8}$ Pa. The Mn- and Ge-deficient Co_2MnGe films were deposited at RT by radio frequency magnetron sputtering from a stoichiometric Co_2MnGe target and subsequently annealed *in situ* at 500 °C for 15 min. The MgO barrier was deposited by electron beam deposition at RT. During this deposition step, the pressure was $\sim 6\times 10^{-7}$ Pa. Finally, an Al layer was deposited by direct current sputtering at RT and a native oxide was formed in an oxygen atmosphere over a period of 2 h. Further details of the sample preparation can be found in Refs. 11 and 12.

X-ray diffraction measurements show that the films grew as epitaxial single-crystal thin films, and the presence of {111} reflections indicate the sample is at least partially $L2_1$ ordered.[29] A high-resolution transmission electron microscopy study of a cross section of similar samples also revealed that the Mn- and Ge-deficient Co_2MnGe films were epitaxial and had very sharp interfaces with MgO.[12] Furthermore, the {111} diffraction spots were also observed by electron diffraction, consistent with $L2_1$ ordering.[12] Using inductively coupled plasma optical emission spectroscopy, the composition of a thin film prepared under the same conditions was determined to be $Co_2Mn_{0.77}Ge_{0.42}$, with an accuracy of 2%–3% for each element.[11,12] We assume the same stoichiometry for the sample studied here. This composition of $Co_2Mn_{0.77}Ge_{0.42}$ is important to understand the defects induced in off-stoichiometric Co_2MnGe films and will be discussed in Sec. III B with respect to the experimentally obtained saturation magnetization for this film.

B. MOKE measurements

All MOKE and BLS measurements described below were preformed at RT.

The sample was mounted on a stage capable of rotating around an axis that is perpendicular to the sample's surface and contained by the plane of light incidence. The measurements were carried out in the longitudinal configuration (i.e., the magnetic field is applied in the sample plane and is parallel to the plane of light incidence). The incident light (laser diode, $\lambda=670$ nm) was plane polarized perpendicular to the plane of light incidence (*s*-polarized light). The sample was oriented such that the edge of the substrate (i.e., the MgO [100] direction) is aligned with the 0° in-plane orientation. That is to say, 0° is along the Co_2MnGe $[1\bar{1}0]$ direction (see Fig. 1). For a given in-plane orientation α (with respect to the magnetic field) of the sample, the Kerr rotation is measured as the applied magnetic field is cycled between ±35 mT. The sample is then rotated by 1°, and another Kerr rotation versus field loop is measured. This procedure is repeated until a loop has been measured for every in-plane orientation through a full rotation of the sample (360°). The field strength of 35 mT was sufficient to magnetically saturate the sample, for all orientations.

C. QMOKE measurements

These measurements were carried out using a MOKE magnetometer equipped with a quadrupole magnet, which is described elsewhere.[23] Only results obtained at perpendicular incidence are shown. Briefly, for a given sample orientation, the Kerr rotation is measured in saturation (50 mT) along eight field directions, each oriented 45° away from one another. The Kerr rotation ϕ_1 is measured along the field labeled H_1, which is oriented at 45° (in a clockwise fashion) from the plane of light incidence on the side of the reflected light beam. The subsequent fields labeled 2–8 are successively found in a clockwise fashion. This procedure is repeated every incremental rotation of 5° through a full rotation of the sample. As will be explained below and is detailed in Refs. 20, 30, and 31, the combination of these eight Kerr rotations ϕ_n allows one to determine the contributions to the MOKE signal that are proportional to the longitudinal component of the magnetization M_L, as well as product terms containing both the longitudinal and the transverse components of the magnetization, M_T.

D. BLS measurements

The BLS measurements were performed in the magnetostatic surface mode geometry, i.e., the magnetic field H was applied parallel to the film surface and perpendicular to the plane of light incidence. A diode-pumped, frequency-doubled $Nd:YVO_4$ laser ($\lambda=532$ nm) was used as a light source. The angle of incidence φ (defined by the direction of the incident light and the sample's normal) and the magnetic field were changed. A more detailed description of this instrument is found in Ref. 32.

Downloaded 15 Mar 2010 to 133.87.26.32. Redistribution subject to AIP license or copyright; see http://jap.aip.org/jap/copyright.jsp

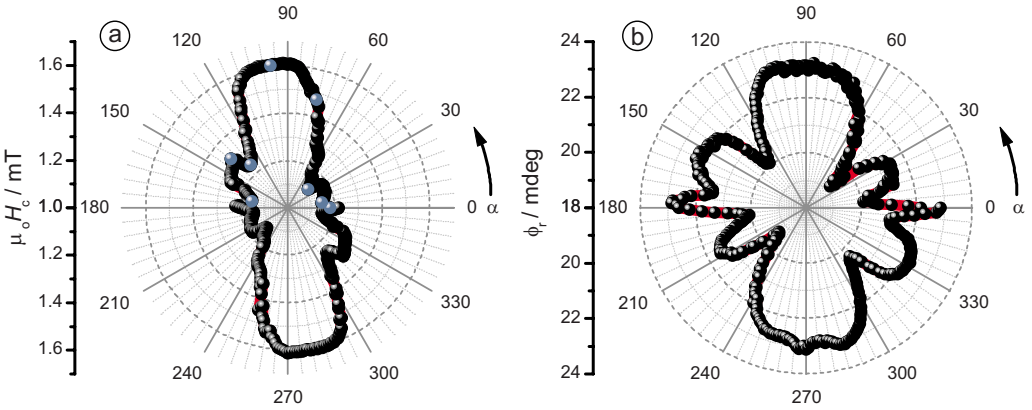

FIG. 2. (Color online) Angular dependence of the coercive field (a) and Kerr rotation at remanence (b) determined by MOKE magnetometry. The angle α is defined by the applied in-plane magnetic field H and the $[1\bar{1}0]$ direction of the Co_2MnGe film. The highlighted data points in (a) correspond to Kerr rotation loops presented in Fig. 3.

Except where specifically indicated, the BLS spectra were recorded at an angle of incidence φ of 45°. For a given angle of incidence, the in-plane wave vector $q_{\parallel}$ of the detected magnons is given by

$$q_{\parallel} = \frac{4\pi}{\lambda}\sin(\varphi). \quad (1)$$

III. RESULTS AND DISCUSSION

A. MOKE magnetometry

The coercive fields determined for each in-plane sample orientation are compiled in Fig. 2(a). We remind that in this figure the 0° orientation corresponds to the Co_2MnGe $[1\bar{1}0]$ orientation (see Fig. 1).

The coercive field $\mu_0 H_c$ ranges between 1.15 and 1.61 mT. The angular dependence clearly displays a uniaxial profile, where the easy axis of magnetization (highest coercive field) is oriented about 7° past the [110] direction (i.e., $\alpha \sim 97°$), and the in-plane hard axis is oriented orthogonally to this direction.

For loops measured at orientations where larger coercivities were observed, for example, at angles of 75° and 97°, as shown in Figs. 3(d) and 3(e), the Kerr rotation loop was quite square, confirming the easy axis character of that orientation. Conversely, loops measured in orientations of lower coercivity showed rounding, which reflects its hard direction character. Such loops can be seen in Figs. 3(b), 3(c), 3(f), and 3(h).

More generally, the Kerr rotation measured in remanence ϕ_r shown in Fig. 2(b) (as well as the reduced remanence ϕ_r/ϕ_{sat}, not shown) shows the same uniaxial behavior as the coercive field shown in Fig. 2(a), with the remanence (and reduced remanence) being maximal along the [110] direction. This again indicates that the easy axis of magnetization is oriented along the [110] direction. The fine structure observed in Fig. 2(a) between 130° and 220° is also more apparent in this graph.

The origin of such uniaxial symmetry may be hard to assess. The small step between our measurements also highlights the rather complex shape of the anisotropy, a feature that is often lost when fewer measurements are performed. To explain the experimental value of the saturation magnetization of 6.43 μ_B/f.u., we tentatively estimated the formula unit composition to be $Co_2[Mn_{0.492}Co_{0.508}][Ge_{0.527}Mn_{0.473}]$, as will be described in Sec. III B, where the first bracket relates to the site occupancy of the Mn site of the ideal $L2_1$ structure,[29] and the second bracket relates to the Ge site occupancy.[29] We speculate that the observed uniaxial symmetry was probably related to the fact that (1) the Ge sites were only half-occupied by Ge atoms in the $Co_2Mn_{0.77}Ge_{0.42}$ film, and (2) a possible preferential distribution of the Ge atoms on the Ge sites is present.

When strains lower than 2% were present, for example, in $Co_2Cr_{0.6}Fe_{0.4}Al$ grown on Fe- or Cr-buffered MgO (Ref. 22) and Co_2MnSi grown on Cr-buffered MgO,[19] we previously observed a very clear fourfold anisotropy, which was indicative of the cubic magnetocrystalline anisotropy of these samples.

Studies of the magnetic properties of single-crystal (001) oriented Co_2MnGe thin films on GaAs(001) have revealed a combination of in-plane fourfold and uniaxial anisotropy.[33,34]

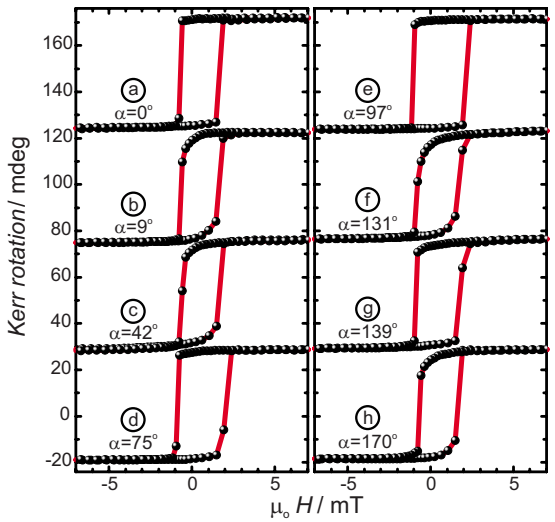

FIG. 3. (Color online) Representative Kerr rotation loops measured in fields of ±35 mT. For clarity, only the region between ±7 mT is shown. The loops correspond to the highlighted points in Fig. 2(a).

Downloaded 15 Mar 2010 to 133.87.26.32. Redistribution subject to AIP license or copyright; see http://jap.aip.org/jap/copyright.jsp

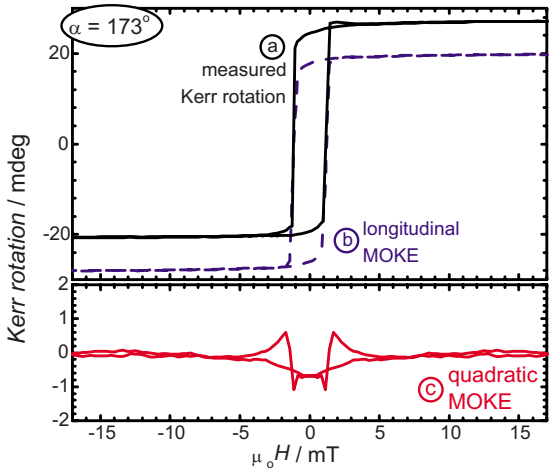

FIG. 4. (Color online) Loop measured at α=173° (a), as well as the extracted longitudinal (b) and quadratic (c) MOKE components of the signal.

However, in both these cases, multistep magnetization reversal was observed, which was attributed to two combined anisotropy (cubic magnetocrystalline anisotropy and surface uniaxial anisotropy) sharing the same easy axis.[34] This is not the case here, as can be seen in Fig. 3 where magnetization reversal is seen to occur in a single step for every orientation.

As can be seen in Fig. 4 for measurements at an in-plane orientation of 173°, the measured Kerr rotation exhibits an asymmetry with respect to an inversion of the magnetic field. The symmetric and asymmetric components of the Kerr signal ϕ may be arithmetically extracted.[20] The two components are given as

$$\mathrm{LMOKE}_{\uparrow\downarrow} \mapsto \phi_{\mathrm{sym}} = \frac{\phi(H_{\uparrow\downarrow}) - \phi(-H_{\downarrow\uparrow})}{2}, \tag{2}$$

$$\mathrm{QMOKE}_{\uparrow\downarrow} \mapsto \phi_{\mathrm{asym}} = \frac{\phi(H_{\uparrow\downarrow}) + \phi(-H_{\downarrow\uparrow})}{2}, \tag{3}$$

where the arrows indicate the branches of the loop with increasing (↑) and decreasing (↓) field strengths. As is indicated, the component that is symmetric upon field inversion is attributed to the longitudinal component of the Kerr signal (LMOKE), and the asymmetric component is attributed to a quadratic component (QMOKE). The origin of QMOKE is not yet fully understood, but the contemporary view places its origin in second-order spin-orbit coupling.[35] The microscopic details leading to the observation of QMOKE in a given sample are not yet firmly established, but QMOKE has been observed in a range of cobalt-based Heusler-compound thin films such as $Co_xMn_yGe_{1-x-y}(111)$,[36,37] $Co_2FeSi(001)$,[20,21] $Co_2MnSi(001)$,[19] and (among other systems) thin Fe films.[30,31,38,39]

To quantify the amplitude of the QMOKE component, we have carried out the "eight field method" (see Sec. II and Refs. 20, 30, and 31 for more details). The eight measured Kerr rotations ϕ_n are combined according to (see Fig. 1 for geometry)

$$\phi_{M_{\mathrm{L}}}^{\mathrm{sat}} = \frac{\phi_8 - \phi_4}{2}, \tag{4}$$

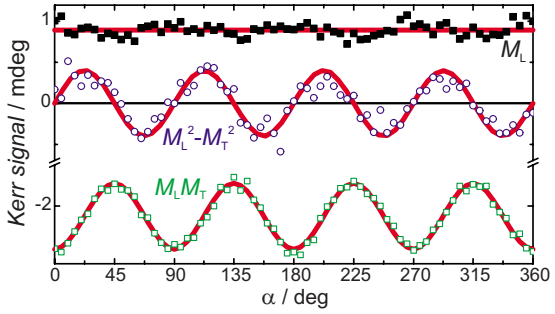

FIG. 5. (Color online) QMOKE measurements, showing longitudinal MOKE signal (■) and the two quadratic terms $M_{\mathrm{L}}^2 - M_{\mathrm{T}}^2$ (○) and $M_{\mathrm{L}}M_{\mathrm{T}}$ (□). Lines are fits to Eq. (7).

$$\phi_{M_{\mathrm{L}}M_{\mathrm{T}}}^{\mathrm{sat}} = \frac{\phi_1 + \phi_5 - \phi_3 - \phi_7}{4}, \tag{5}$$

$$\phi_{M_{\mathrm{L}}^2 - M_{\mathrm{T}}^2}^{\mathrm{sat}} = \frac{\phi_8 + \phi_4 - \phi_2 - \phi_6}{4}, \tag{6}$$

and yield the LMOKE signal in saturation $\phi_{M_{\mathrm{L}}}^{\mathrm{sat}}$ as well as two QMOKE signals $\phi_{M_{\mathrm{L}}M_{\mathrm{T}}}^{\mathrm{sat}}$ and $\phi_{M_{\mathrm{L}}^2 - M_{\mathrm{T}}^2}^{\mathrm{sat}}$. The measured signals are presented in Fig. 5 as a function of in-plane sample orientation. As can be seen, the LMOKE does not depend on the sample direction. The two QMOKE signals exhibit a sinusoidal behavior, and both have the same amplitude (0.4 mdeg in this case) and the MOKE signal proportional to $M_{\mathrm{L}}M_{\mathrm{T}}$ is vertically offset from zero. This amplitude, while clearly observed experimentally due to our sensitive experimental setup,[23] is quite modest. For comparison, amplitudes of ~2 and ~18 mdeg were observed for Co_2MnSi (Ref. 23) and Co_2FeSi (Ref. 20) thin films, respectively.

The expected Kerr rotation for a cubic material, when taking into account effects up to the second order of the magnetization,[31] is the real part of

$$\Phi_{\mathrm{s}} = \mathcal{A} \cdot KM_{\mathrm{L}} + \mathcal{B}\left[\left(-\frac{K^2}{\tilde{n}^2} + 2G_{44} + \frac{\Delta G}{2}\right)M_{\mathrm{L}}M_{\mathrm{T}} - \frac{\Delta G}{2}\cos 4\alpha \cdot M_{\mathrm{L}}M_{\mathrm{T}} - \frac{\Delta G}{4}\sin 4\alpha (M_{\mathrm{L}}^2 - M_{\mathrm{T}}^2)\right], \tag{7}$$

where $\mathcal{A}$ and $\mathcal{B}$ are the (complex) optical weighting factors,[40] K and G_{ij} are the components of the linear and quadratic magneto-optical tensors, respectively, $\Delta G = G_{11} - G_{12} - 2G_{44}$ embodies the magneto-optical anisotropy, and $\tilde{n}$ is the complex refractive index of the material. The salient features of Eq. (7) are recognized in the data shown in Fig. 5. This suggests that the electronic properties of this sample are well described by a cubic environment, as expected for a Heusler compound.[19–23] The solid lines in Fig. 5 are fits to the various components of Eq. (7).

B. BLS spectroscopy

BLS spectra were measured in various magnetic fields, as is shown in Fig. 6(a). The positions of the observed peaks shift to larger absolute frequencies with increasing field. This

Downloaded 15 Mar 2010 to 133.87.26.32. Redistribution subject to AIP license or copyright; see http://jap.aip.org/jap/copyright.jsp

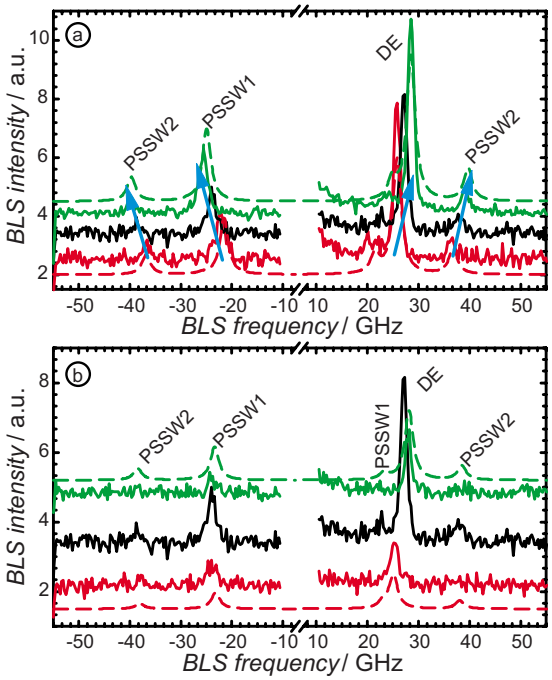

FIG. 6. (Color online) (a) BLS spectra measured in various applied magnetic field strengths ($\mu_0 H$=170, 215, and 260 mT from bottom to top) at φ=45°. (b) BLS spectra measured at various angles of incidence (φ=25°, 45°, and 65° from bottom to top) in an applied field of 215 mT. In both (a) and (b), the dashed lines represent the calculated spectra (see text).

is evidence that these peaks are of magnonic origin, as peaks arising from phonons would not be shifted by an applied magnetic field.[41]

The Damon–Esbach mode (dipole-dominated magnetostatic surface mode, i.e., $q \perp M_s$) can be discriminated from the perpendicular standing spin-wave (PSSW) mode by changing the angle of incidence. For the former (neglecting exchange), the spin-wave frequency ω_{DE} is given in Système International units by

$$\omega_{DE} = \gamma\mu_0 \sqrt{H(H+M_s) + \frac{M_s^2}{8\pi}\{1 - e^{-2q_{\parallel}d}\}}, \tag{8}$$

where $\gamma = (1/g_e)|\gamma_e|g$ is the gyromagnetic ratio (γ_e is the gyromagnetic ratio of a free electron, and g_e and g are and the Landé factors for the free electron and the material, respectively), μ_0 is the permeability of vacuum, M_s is the saturation magnetization[42] (assumed to be aligned with the applied field H), and d is the film thickness.

For the nth PSSW mode, the wave vector q_n is quantized according to

$$q_n = n\frac{\pi}{d}, \tag{9}$$

where n is an integer, and the observed frequency can be approximated as

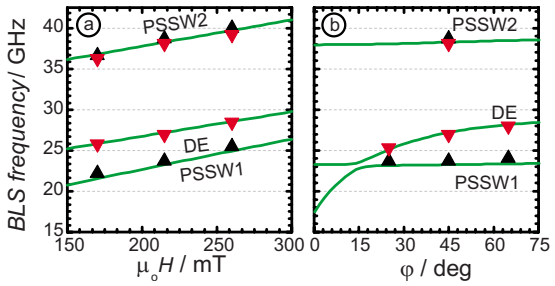

FIG. 7. (Color online) Calculated magnon dispersion for the Damond–Esbach and the PSSW as function of (a) applied magnetic field (φ=45°) and (b) angle of incidence ($\mu_0 H$=215 mT). In both panels, the experimentally observed spin-wave frequencies are also provided (▲=Stokes and ▼=anti-Stokes lines).

$$\omega_{PSSW} = \gamma\mu_0 \sqrt{\left(H + \frac{2A}{\mu_0 M_s}q_n^2\right)\left(H + M_s + \frac{2A}{\mu_0 M_s}q_n^2\right)}, \tag{10}$$

where the exchange constant A is introduced. These PSSW modes are thus rather insensitive to the angle of incidence.[43]

Figure 6(b) shows the BLS spectra measured at various angles of incidence. The peaks near 26 GHz clearly shift position upon varying the angle of incidence, marking them as the DE modes. Conversely, the other observed peaks are assigned to the PSSW modes.

Using a model by Hillebrands[44] based on a continuum-type magnetostatic theory, the exchange constant A, the related spin-wave stiffness $D = [2g\mu_B]/[AM_s]$ (μ_B being the Bohr magneton),[25] the saturation magnetization, and the Landé g-factor can be determined from the experimentally observed spin-wave frequencies. Figure 7 shows the calculated dispersions for $A = 22.5 \pm 1.0$ pJ/m ($D = 413 \pm 15$ meV Å^2), $\mu_0 M_s = 1.58 \pm 0.05$ T (6.43 μ_B/f.u.), and $g = 2.0 \pm 0.1$. As can be seen, these dispersions show a very good agreement with the observed spin-wave frequencies.

The exchange constant A we determine (22.5 pJ/m) is approximately twice as large as the values reported for Co_2MnGe(110) films grown on Al_2O_3 by Belmeguenai *et al.*[27,28] In those studies, A was found to vary between 9.8 and 13.8 pJ/m for film thickness ranging from 30 to 83 nm. A discrepancy of this order is not surprising, as the exchange constant was shown to be dependent on the ordering[19] and the number of valence electrons (i.e., composition).[45] These two physical attributes are likely to be different between the samples studied by Belmeguenai and co-workers and the one studied here.

The effect of point defects on the half-metallicity and saturation magnetization have been studied by means of *ab initio* calculations for $Co_{2\pm x}Mn_{1\mp x}Ge$ (Refs. 46–49) and $Co_2Mn_{1+x}Ge_{1-x}$ (Ref. 50) compounds. While Co_{Mn} antisites, where a Mn site is replaced by a Co atom, destroy half-metallicity,[46–48] this important feature is preserved for Mn_{Co} antisites.[47–49]

Slater–Pauling behavior relates the magnetic moment m per formula unit (or strictly speaking, per unit formula for a

Downloaded 15 Mar 2010 to 133.87.26.32. Redistribution subject to AIP license or copyright; see http://jap.aip.org/jap/copyright.jsp

nonstoichiometric material, including vacancies) to the number of valence electrons N_v in the formula unit by the simple relationship,[51]

$$m = N_v - 24.$$

This behavior is expected for half-metallic ferromagnets,[51] and predicted to remain valid for $Co_2Mn_{1+x}Ge_{1-x}$ for $-0.2 < x < 0.2$,[50] It is worth mentioning that this feature is also maintained for closely related Mn-rich Co_2MnSi compounds.[52] We will now discuss a possible formula unit composition of the $Co_2Mn_{0.77}Ge_{0.42}$ films based on this extended Slater–Pauling behavior as an approximation for the Co–rich, Ge–deficient Co_2MnGe samples studied here along with taking into consideration the influence of Co_{Mn} antisites involved in the possible formula unit composition.

According to the theoretically calculated energies of formation ΔE for various kinds of defects in Co_2MnSi,[52] ΔE for a Co_{Mn} antisite (0.75 eV), where a Mn site is replaced by a Co atom, is much smaller than ΔE for a Co_{Si} antisite (2.25 eV), ΔE for a vacancy at a Mn site (1.43 eV), and ΔE for a vacancy at a Si site (3.74 eV). By assuming a similar tendency in ΔE for defects in Co_2MnGe,[47] Co_{Mn} antisites are likely to be induced for Mn- and Ge-deficient $Co_2Mn_{0.77}Ge_{0.42}$. If we tentatively describe the formula unit composition to be $Co_2[Mn_{0.83}Co_{0.17}]Ge_{0.455}$, where Co_{Mn} antisites are induced and the Ge sites are approximately half-occupied, this tentative formula unit composition provides a Slater–Pauling M_s value of 3.15 μ_B/f.u., which is much smaller than the M_s value of 6.43 μ_B/f.u. measured by the BLS spectroscopy.

Alternatively, if we describe the formula unit composition to be $Co_2[Mn_{0.492}Co_{0.508}][Ge_{0.527}Mn_{0.473}]$, where all the Co, Mn and Ge sites are fully occupied and the formation of Co_{Mn} and Mn_{Ge} antisites are assumed [note that ΔE for a Mn_{Si} antisite (1.69 eV) is much smaller than ΔE for a Co_{Si} antisite (2.25 eV) for Co_2MnSi (Ref. 52)], this tentative formula unit composition provides a Slater–Pauling M_s value of 7.44 μ_B/f.u., which is closer to the M_s value of 6.43 μ_B/f.u. measured by BLS spectroscopy. Furthermore, this formula unit model featuring all the Co, Mn, and Ge sites being fully occupied is reasonable if we take into consideration that any ΔE values for vacancies at a Co site, a Mn site and a Si site are much higher than ΔE for a Co_{Mn} antisite and a Mn_{Si} antisite in the case of Co_2MnSi.[52] The lower experimental M_s (6.43 μ_B/f.u.) than the Slater-Pauling M_s value (7.44 μ_B/f.u.) is also reasonable if we consider that a Co_{Mn} antisite decreases the magnetic moment of the formula unit as theoretically predicted.[47] Alternatively, it can be attributed to the possible existence of a small amount of vacancies at the Co, Mn, or Ge site. Taking into account the theoretical prediction that a vacancy at a Co site has a lower ΔE than a vacancy at a Mn site and a vacancy at a Si site in Co_2MnSi,[52] vacancies are more likely to be introduced at Co sites in Co_2MnGe.

Given these considerations, we assume a possible formula unit composition of $Co_{1.87}\square_{0.13}[Mn_{0.44}Co_{0.56}] \times [Ge_{0.51}Mn_{0.49}]$, where the formation of Co_{Mn} antisites, Mn_{Ge} antisites, and vacancies at Co sites ($\square$) are assumed. This formula unit composition provides a number of valence electrons per formula unit (N_v) of 30.4. This N_v, assuming the generalized Slater–Pauling rule for the Mn- and Ge-deficient Co_2MnGe films, provides a M_s value of 6.4 μ_B/f.u. (note that the composition of $Co_{1.87}\square_{0.13}[Mn_{0.44}Co_{0.56}][Ge_{0.51}Mn_{0.49}]$ is identical to the description of the film composition of $Co_2Mn_{0.77}Ge_{0.42}$). Again, the first and second brackets describe the site occupancy of the Mn and Ge sites of the ideal $L2_1$ structure, respectively.[29] The saturation magnetization of 6.4 μ_B/f.u. thus calculated reproduces well the experimental M_s value of 6.43 μ_B/f.u. However, it neglects the reduction of M_s theoretically predicted for Co_{Mn} antisites,[47] and would provide an upper limit as to the occurrence of Co vacancies. The good agreement suggests that Co_{Mn} antisites are induced and the Ge sites are partially occupied by Mn atoms.

In summary, it is worth to highlight the contrast between the results observed by both MOKE techniques presented above. The rotational scan clearly points to uniaxial symmetry (Fig. 2) and may be due to the atomic ordering of the nonstoichiometric system. On the other hand, the QMOKE measurements in saturation are in full agreement with the magneto-optical tensor for a material with cubic symmetry. The perturbation leading to the observed complex uniaxial anisotropy of the magnetization reversal processes (see Fig. 2) apparently has little influence on the electronic structure of the material, in particular, with respect to the anisotropy of the spin-orbit coupling (see Fig. 5 and related discussion).

IV. CONCLUSION

We have examined an epitaxial, nonstoichiometric Mn- and Ge-deficient $Co_2Mn_{0.77}Ge_{0.42}$ thin films by means of MOKE magnetometry and BLS spectroscopy. We find the sample exhibits a unidirectional anisotropy. A modest quadratic MOKE with an amplitude of 0.4 mdeg is observed. Using BLS spectroscopy, we find the exchange constant $A = 22.5$ pJ/m (exchange stiffness $D = 413$ meV Å^2), which is twice higher than previously reported for $Co_2MnGe(110)$ films.[27,28] Even though the composition is highly off-stoichiometric, the magnetic moment appears to be approximated by Slater–Pauling behavior. Furthermore, while the magnetization reversal shows a clear uniaxial symmetry, the magneto-optical tensor describing this material is not significantly perturbed with respect to the ideal cubic symmetry.

ACKNOWLEDGMENTS

We thank Dr. J. Lösch (IFOS, TU Kaiserslautern) for x-ray measurements. We also thank Associate Professor T. Uemura (Hokkaido University) for helpful discussions. This project was financially supported by the DFG Research Unit 559, "New Materials with High Spin Polarization" (Germany). S.T. gratefully acknowledges the Alexander von Humboldt foundation for a postdoctoral research fellowship. This work was partly supported by a Grant-in-Aid for Scientific Research (A) (Grant No. 20246054), a Grant-in-Aid for Scientific Research on Priority Area "Creation and control of spin current" (Grant No. 19048001), and a Grant-in-aid for Hokkaido Innovation through Nanotechnology Support (HINTS) from the MEXT (Japan).

Downloaded 15 Mar 2010 to 133.87.26.32. Redistribution subject to AIP license or copyright; see http://jap.aip.org/jap/copyright.jsp

[1]S. Fujii, S. Sugimura, S. Ishida, and S. Asano, J. Phys. Condens. Matter **2**, 8583 (1990).
[2]S. Ishida, S. Fujii, S. Kashiwagi, and S. Asano, J. Phys. Soc. Jpn. **64**, 2152 (1995).
[3]S. Picozzi, A. Continenza, and A. Freeman, Phys. Rev. B **66**, 094421 (2002).
[4]I. Galanakis, P. Mavropoulos, and P. H. Dederichs, J. Phys. D: Appl. Phys. **39**, 765 (2006).
[5]P. J. Webster, J. Phys. Chem. Solids **32**, 1221 (1971).
[6]T. Marukame, T. Kasahara, K.-i. Matsuda, T. Uemura, and M. Yamamoto, Jpn. J. Appl. Phys., Part 2 **44**, L521 (2005).
[7]M. Yamamoto, T. Marukame, T. Ishikawa, K.-i. Matsuda, T. Uemura, and M. Arita, J. Phys. D: Appl. Phys. **39**, 824 (2006).
[8]T. Ishikawa, T. Marukame, H. Kijima, K.-i. Matsuda, T. Uemura, M. Arita, and M. Yamamoto, Appl. Phys. Lett. **89**, 192505 (2006).
[9]T. Ishikawa, S. Hakamata, K.-i. Matsuda, T. Uemura, and M. Yamamoto, J. Appl. Phys. **103**, 07A919 (2008).
[10]T. Ishikawa, N. Itabashi, T. Taira, K.-i. Matsuda, T. Uemura, and M. Yamamoto, J. Appl. Phys. **105**, 07B110 (2009).
[11]T. Taira, T. Ishikawa, N. Itabashi, K.-i. Matsuda, T. Uemura, and M. Yamamoto, Appl. Phys. Lett. **94**, 072510 (2009).
[12]T. Taira, T. Ishikawa, N. Itabashi, K.-i. Matsuda, T. Uemura, and M. Yamamoto, J. Phys. D: Appl. Phys. **42**, 084015 (2009).
[13]T. Ishikawa, H.–x. Liu, T. Taira, K.-i. Matsuda, T. Uemura, and M. Yamamoto, Appl. Phys. Lett. **95**, 232512 (2009).
[14]R. Shan, H. Sukegawa, W. H. Wang, M. Kodzuka, T. Furubayashi, T. Ohkubo, S. Mitani, K. Inomata, and K. Hono, Phys. Rev. Lett. **102**, 246601 (2009).
[15]T. Marukame and M. Yamamoto, J. Appl. Phys. **101**, 083906 (2007).
[16]T. Ishikawa, N. Itabashi, T. Taira, K.-i. Matsuda, T. Uemura, and M. Yamamoto, Appl. Phys. Lett. **94**, 092503 (2009).
[17]V. Drewello, J. Schmalhorst, A. Thomas, and G. Reiss, Phys. Rev. B **77**, 014440 (2008).
[18]P. Mavropoulos, M. Ležaić, and S. Blügel, Phys. Rev. B **72**, 174428 (2005).
[19]O. Gaier, J. Hamrle, S. J. Hermsdoerfer, H. Schultheiß, B. Hillebrands, Y. Sakuraba, M. Oogane, and Y. Ando, J. Appl. Phys. **103**, 103910 (2008).
[20]J. Hamrle, S. Blomeier, O. Gaier, B. Hillebrands, K. Postava, H. Schneider, G. Jakob, and C. Felser, J. Phys. D: Appl. Phys. **40**, 1563 (2007).
[21]J. Hamrle, S. Blomeier, O. Gaier, B. Reuscher, A. Brodyanski, M. Kopnarski, K. Postava, H. Schneider, G. Jakob, C. Felser, and B. Hillebrands, J. Phys. D: Appl. Phys. **40**, 1558 (2007).
[22]J. Hamrle, S. Blomeier, O. Gaier, B. Hillebrands, R. Schäfer, and M. Jourdan, J. Appl. Phys. **100**, 103904 (2006).
[23]S. Trudel, G. Wolf, H. Schultheiss, J. Hamrle, B. Hillebrands, T. Kubota, and Y. Ando, Rev. Sci. Instrum. **81**, 026105 (2010).
[24]O. Gaier, J. Hamrle, S. Trudel, B. Hillebrands, H. Schneider, and G. Jakob, J. Phys. D: Appl. Phys. **42**, 232001 (2009).
[25]J. Hamrle, O. Gaier, S.-G. Min, B. Hillebrands, Y. Sakuraba, and Y. Ando, J. Phys. D: Appl. Phys. **42**, 084005 (2009).
[26]O. Gaier, J. Hamrle, S. Trudel, A. Conca Parra, B. Hillebrands, E. Arbelo, C. Herbort, and M. Jourdan, J. Phys. D: Appl. Phys. **42**, 084004 (2009).
[27]M. Belmeguenai, F. Zighem, G. Woltersdorf, Y. Roussigné, S. M. Chérif, K. Westerholt, and G. Bayreuther, J. Magn. Magn. Mater. **321**, 750 (2009).
[28]M. Belmeguenai, F. Zighem, Y. Roussigné, S.-M. Chérif, P. Moch, K. Westerholt, G. Woltersdorf, and G. Bayreuther, Phys. Rev. B **79**, 024419 (2009).
[29]The $L2_1$ structure for a $M_2M'Z$ full-Heusler compound is described by the $Fm\bar{3}m/225$ space group. The M atoms occupy the Wyckoff 8c positions $(\frac{1}{4},\frac{1}{4},\frac{1}{4})$, while the M' and Z atoms are located at the 4a (0,0,0) and 4b $(\frac{1}{2},\frac{1}{2},\frac{1}{2})$ positions, respectively.
[30]K. Postava, H. Jaffres, A. Schuhl, F. N. V. Dau, M. Goiran, and A. R. Fert, J. Magn. Magn. Mater. **172**, 199 (1997).
[31]K. Postava, D. Hrabovský, J. Pištora, A. R. Fert, Š. Višňovský, and T. Yamaguchi, J. Appl. Phys. **91**, 7293 (2002).
[32]B. Hillebrands, Rev. Sci. Instrum. **70**, 1589 (1999).
[33]T. Ambrose, J. J. Krebs, and G. A. Prinz, Appl. Phys. Lett. **76**, 3280 (2000).
[34]F. Y. Yang, C. H. Shang, C. L. Chien, T. Ambrose, J. J. Krebs, G. A. Prinz, V. I. Nikitenko, V. S. Gornakov, A. J. Shapiro, and R. D. Shull, Phys. Rev. B **65**, 174410 (2002).
[35]R. M. Osgood III, S. D. Bader, B. M. Clemens, R. L. White, and H. Matsuyama, J. Magn. Magn. Mater. **182**, 297 (1998).
[36]P. K. Muduli, W. C. Rice, L. He, and F. Tsui, J. Magn. Magn. Mater. **320**, L141 (2008).
[37]P. K. Muduli, W. C. Rice, L. He, B. A. Collins, Y. S. Chu, and F. Tsui, J. Phys.: Condens. Matter **21**, 296005 (2009).
[38]S. S. Yan, R. Schreiber, P. Grünberg, and R. Schäfer, J. Magn. Magn. Mater. **210**, 309 (2000).
[39]M. Buchmeier, R. Schreiber, D. E. Bürgler, and C. M. Schneider, Phys. Rev. B **79**, 064402 (2009).
[40]At normal incidence, $\mathcal{A}=(\tilde{n}_o^2\varphi)/[\tilde{n}^2(\tilde{n}_o^2-\tilde{n}^2)]$ and $\mathcal{B}=\tilde{n}_o/[\tilde{n}(\tilde{n}_o^2-\tilde{n}^2)]$, where φ is the angle of incidence and $\tilde{n}$ and $\tilde{n}_o$ are the complex refractive indices of the material and the incident medium, respectively. This neglects the AlO_x capping layer, the MgO barrier, and the finite thickness of the magneto-optically active film.
[41]B. Hillebrands, in *Light Scattering in Solids VII*, edited by M. Cardona and G. Güntherodt (Springer-Verlag, Heidelberg, 2000).
[42]Note that we determine the volume magnetization saturation, which we then convert to a magnetization per unit cell.
[43]B. Hillebrands, in *Modern Techniques for Characterizing Magnetic Materials*, edited by Y. Zhu (Kluwer Academic, Boston, 2005).
[44]B. Hillebrands, Phys. Rev. B **41**, 530 (1990).
[45]J. Hamrle, S. Trudel, O. Gaier, and B. Hillebrands (unpublished).
[46]S. Picozzi, A. Continenza, and A. J. Freeman, J. Appl. Phys. **94**, 4723 (2003).
[47]S. Picozzi, A. Continenza, and A. J. Freeman, Phys. Rev. B **69**, 094423 (2004).
[48]S. Picozzi and A. J. Freeman, J. Phys.: Condens. Matter **19**, 315215 (2007).
[49]K. Özdoğan, I. Galanakis, E. Şaşioğlu, and B. Aktaş, Solid State Commun. **142**, 492 (2007).
[50]I. Galanakis, K. Özdoğan, B. Aktaş, and E. Şaşioğlu, Appl. Phys. Lett. **89**, 042502 (2006).
[51]I. Galanakis, P. H. Dederichs, and N. Papanikolaou, Phys. Rev. B **66**, 174429 (2002).
[52]B. Hülsen, M. Scheffler, and P. Kratzer, Phys. Rev. B **79**, 094407 (2009).

Downloaded 15 Mar 2010 to 133.87.26.32. Redistribution subject to AIP license or copyright; see http://jap.aip.org/jap/copyright.jsp